Supplementary Materials

Section S1: Supplementary Materials and Methods

S1.1. Model parameters

We approximated the model parameter values from the literature as follows. From the average lifetime of PCs of 2.3 min [1], we fixed the PC disassembly rate constant, d, to be 0.4 min^{-1}. From the average number of point contacts per growth cone of ~ 9 [1], the PC assembly rate constant was approximated as $a \sim 9d \sim 3.6$ min^{-1}, and we assumed $x = 0.05$. In our model, factors involved in PC assembly, such as the density and nature of ECM, expression levels of integrin receptor, interactions between ECM ligand and integrin receptors and subsequent receptor clustering, and recruitment of adapter and signalling proteins, are lumped into the PC adhesion assembly rate constant. Any changes in the extracellular conditions, for example, changes in the density of ECM, and in the expression and activity levels of proteins involved in the PC assembly will alter a in our model. We have therefore varied a between 1 and 5 min^{-1}. Following the literature [2-4], we fixed the Rac1 activation rate constant, $k_{a\mathrm{r}}$, to be 9 min^{-1}, the Rac1 deactivation rate constant, $k_{d\mathrm{r}}$, to be 3 min^{-1}, and the total number of Rac1 molecules in the growth cone, R_{1T}, to be 1000. We chose the baseline values of b_0 to be 0.1 min^{-1}, K_{R1} to be 400 molecules per growth cone, and K_N to be 3 per growth cone.

We explored the model behaviour with ultrasensitivity in the positive feedback loop by fixing Hill coefficients h_1 and h_2 to be 3 and without ultrasensitivity by fixing h_1 and h_2 to be 1. Although there is currently no quantitative data available to estimate the Hill coefficients in this system, several mechanisms could generate ultrasensitivity in the multistep Rac1-mediated PC assembly and PC-dependent Rac1 activation [5-7]. One possible source of ultrsensitivity is through additional positive feedback loops in this multistep process [6]. PXN in PCs recruits PIX to activate Rac1. Phosphorylation of PXN at serine 273 enhances PIX recruitment. Active Rac1 mediates phosphorylation of PAK, which in turn phosphorylates of PXN at serine 273. Thus, PC-mediated Rac1 activation consist of a positive feedback loop. The clustering of integrin receptors,

which is required for growth cone PC formation [8], has been suggested to be regulated by positive feedback mechanisms [9, 10]. Another possibility is that cooperativity in the multistep processes involved in PC adhesion dynamics could contribute to ultrasensitivity. The membrane recruitment process of many proteins, such as N-WASP and PAK1, clustering of focal adhesion proteins, such as FAK, and recruitment of PXN to focal adhesions appear to display cooperativity in other biological systems [11-14]. It is thus conceivable that cooperativity in the molecular steps involved in the growth cone PC adhesion dynamics could generate ultrasensitive responses.

S1.2. Deterministic model solution

We solved the model using the fsolve routine in MATLAB to determine the null clines in figure 1. We also obtained the steady state values of the model using the NSolve routine in Mathematica.

S1.3. Stochastic simulations

We performed stochastic simulations of the model using Gillespie's direct method implemented in MATLAB. We obtained the steady state distribution from a 10^6 min simulation trace, with samples taken over a constant time interval of 0.05 min [15]. When the deterministic model exhibited bistability, the first passage time was computed by initialising the model variables (R_1 and N) with values corresponding to one of the steady states and by estimating the time required for the model variables to reach the values of the other steady state for the first time. When the deterministic model admitted only one stable steady state and the model growth cone displayed switching behaviour, the first passage time was computed by estimating the time required for the system to switch from the monostable steady state values to basal levels of active Rac1 and zero point contacts for the first time, and vice versa.

Section S2: Supplementary Figures

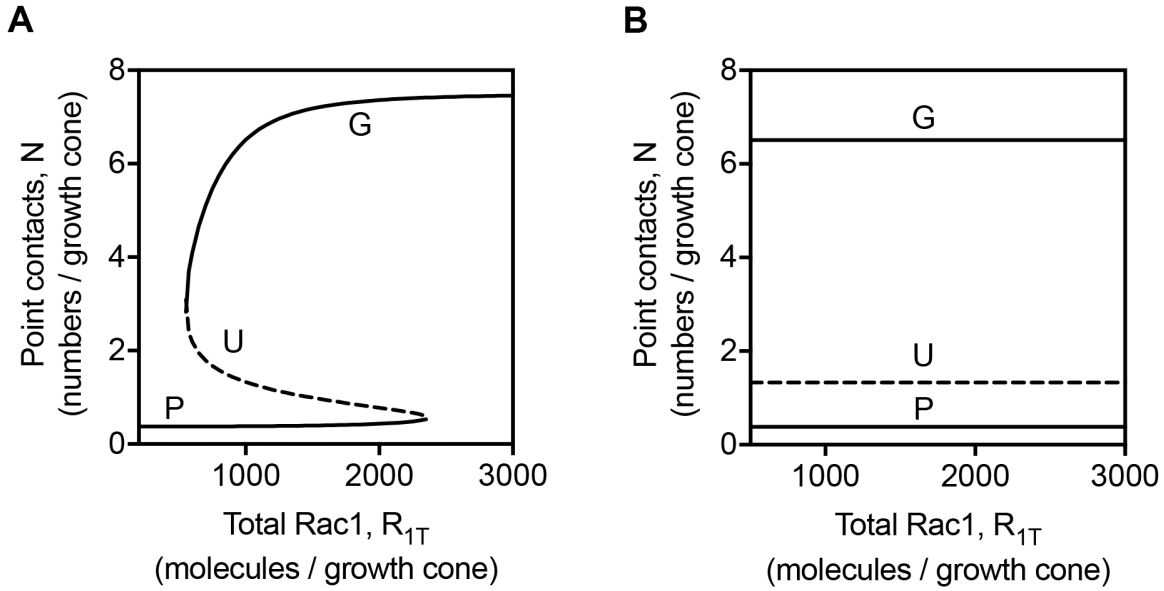

Figure S1. Dependence of steady states of the system on the total Rac1 molecules in a growth cone. Steady state values of the number of point contacts as a function of the total number of Rac1 molecules in a growth cone, R_{1T}, with **(A)** a fixed value of activation coefficient K_{R1} = 400 molecules per growth cone and **(B)** varying values of activation coefficient K_{R1} = 0.4 R_{1T}. G is the growth stable steady state, P is the paused stable steady state and U is the unstable steady state. The other model parameter values are the same as in the Table S1.

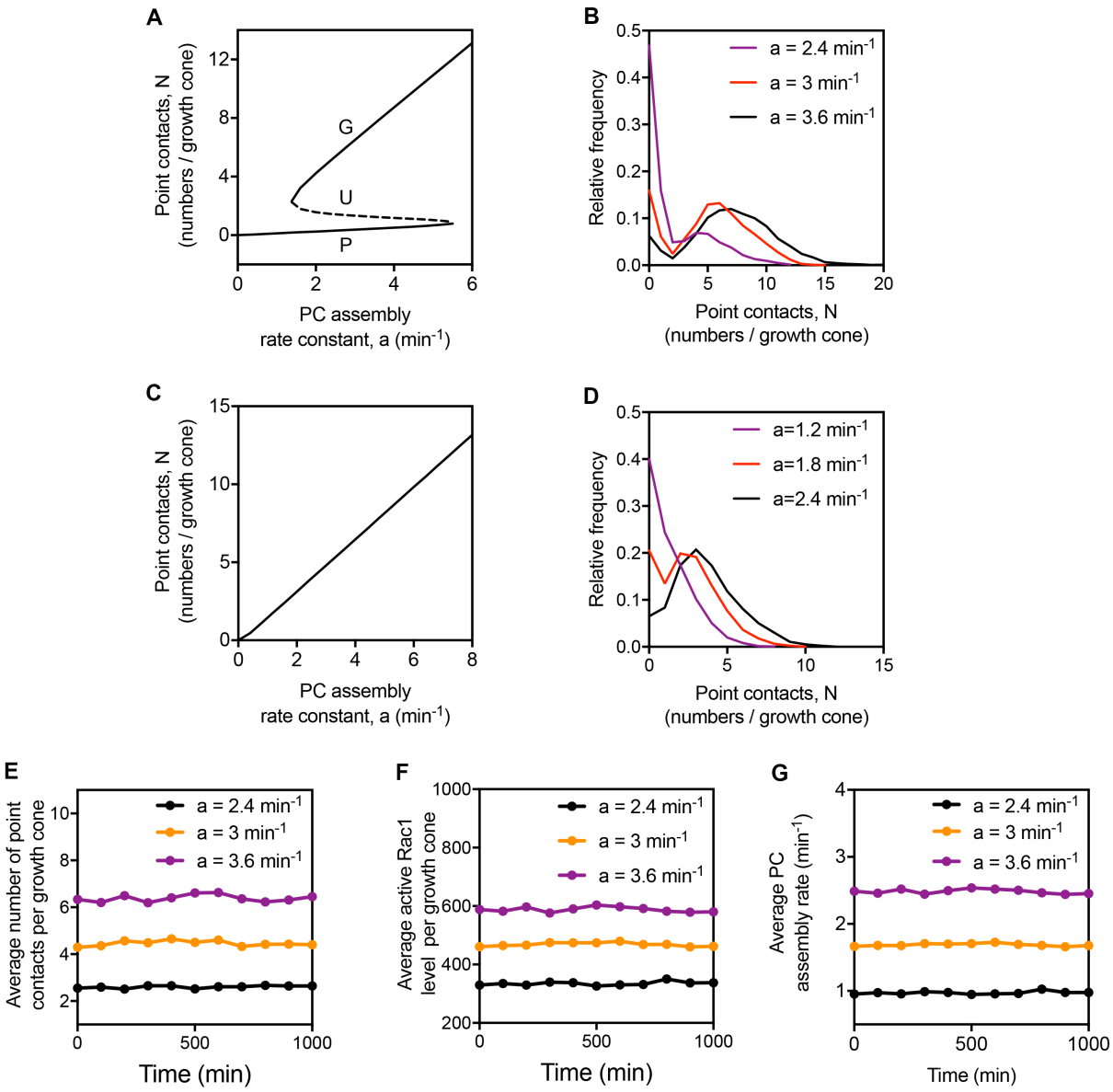

Figure S2. Influence of extracellular signals. (A) Steady state values of the number of point contacts, N, for different values of PC assembly rate constant, a, with $h_1 = h_2 = 3$. G is the growth stable steady state, P is the paused stable steady state and U is the unstable steady state. **(B)** Steady state distributions of N for different values of a with $h_1 = h_2 = 3$. **(C)** Steady state values of N for different values of a with $h_1 = h_2 = 1$. **(D)** Steady state distributions of N for different values of a with $h_1 = h_2 = 1$. **(E)** The number of point contacts, **(F)** the levels of active Rac1 and **(G)** PC assembly rate averaged across 1,000 growth cones for different baseline values of a. In E and F, the parameter set for each growth cone was generated by randomly varying parameter values up to ± 25% from the baseline values. The other model parameter values are the same as in the Table S1.

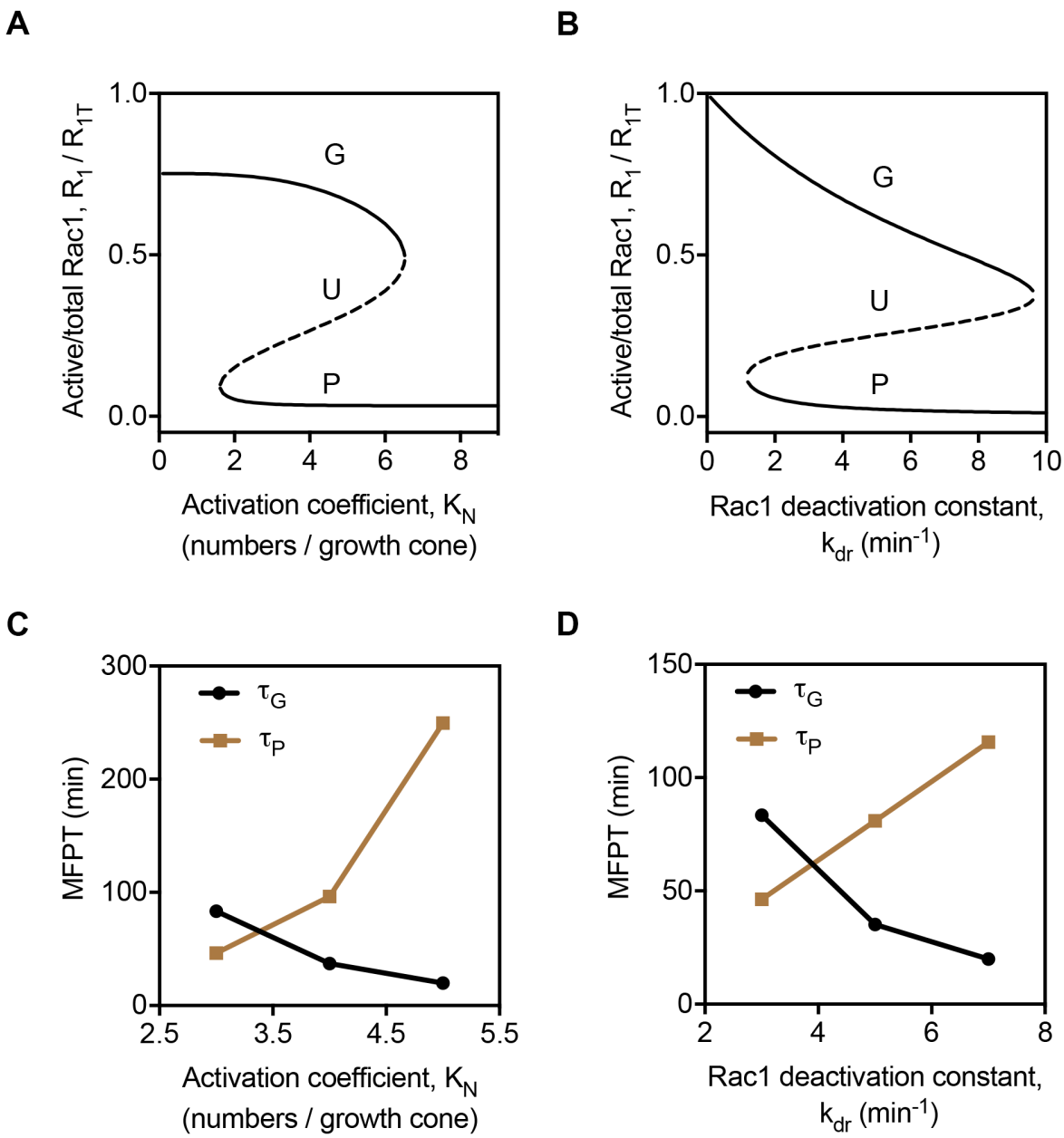

Figure S3. Parameter sensitivity. Steady state values of the levels of active Rac1 for different values of **(A)** activation coefficient, K_N, and **(B)** Rac1 deactivation rate constant, k_{dr}. The MFPTs for different values of **(A)** K_N and **(B)** k_{dr}. τ_G and τ_P are the MFPTs for the growth and paused states, respectively. In A-D, $h_1 = h_2 = 3$. The other model parameter values are the same as in the Table S1.

Section S3: Supplementary Tables

Table S1. Baseline values of model parameters

Parameter	Description	Baseline Value	Unit	Source
a	Point contact assembly rate constant	3	min^{-1}	[1]
x	Factor determining the dependence of PC assembly rate on the active Rac1 levels	0.05	-	Assumed
d	Point contact disassembly rate constant	0.4	min^{-1}	[1]
K_{R1}	Activation coefficient	400	Molecules per growth cone	Assumed
b_0	Basal Rac1 activation rate constant	0.1	min^{-1}	Assumed
k_{ar}	Point contact-dependent Rac1 activation constant	9	min^{-1}	[2]
k_{dr}	Rac1 deactivation rate constant	3	min^{-1}	[2, 4]
K_N	Activation coefficient	3	Numbers per growth cone	Assumed
R_{1T}	Total number of Rac1	1000	Molecules per growth cone	[3]
h_1, h_2	Hill coefficients	1 or 3	-	Assumed

Table S2. Summary of published experimental measurements of time spent by the growth cones in growth and paused states

Experimental system	Growth cone state	Duration	Source
Superior cervical ganglion neurons (cell culture)	Growth	20 to 90 min	[16]
	Paused	10 to 20 min	
Cortical neurons (cell culture)	Paused	1 to 30 h	[17]
Retinal ganglion neurons (chick embryo retina)	Growth	6 to 8 min	[18]
	Paused	4 to 6 min	
Retinal ganglion neurons (mouse brain)	Growth	20 to 90 min	[19]
	Paused	15 to 60 min	
Callosal neurons (hamster brain slice)	Paused	2 to 38 min	[20]
Retinal axons (mouse brain)	Paused	15 to 300 min	[21]
Thalamocortical neurons (internal capsule of rat brain slice)	Paused	5 to 50 min	[22]

Section S4: Supplementary References

1. Woo S., Gomez T.M. 2006 Rac1 and RhoA promote neurite outgrowth through formation and stabilization of growth cone point contacts. *J Neurosci* **26**(5), 1418-1428. (doi:10.1523/JNEUROSCI.4209-05.2006).

2. Huang B., Lu M., Jolly M.K., Tsarfaty I., Onuchic J., Ben-Jacob E. 2014 The three-way switch operation of Rac1/RhoA GTPase-based circuit controlling amoeboid-hybrid-mesenchymal transition. *Sci Rep* **4**, 6449. (doi:10.1038/srep06449).

3. Zeitz M., Kierfeld J. 2014 Feedback mechanism for microtubule length regulation by stathmin gradients. *Biophys J* **107**(12), 2860-2871. (doi:10.1016/j.bpj.2014.10.056).

4. Cirit M., Krajcovic M., Choi C.K., Welf E.S., Horwitz A.F., Haugh J.M. 2010 Stochastic model of integrin-mediated signaling and adhesion dynamics at the leading edges of migrating cells. *PLoS Comput Biol* **6**(2), e1000688. (doi:10.1371/journal.pcbi.1000688).

5. Ferrell J.E., Jr., Ha S.H. 2014 Ultrasensitivity part I: Michaelian responses and zero-order ultrasensitivity. *Trends Biochem Sci* **39**(10), 496-503. (doi:10.1016/j.tibs.2014.08.003).

6. Ferrell J.E., Jr., Ha S.H. 2014 Ultrasensitivity part II: multisite phosphorylation, stoichiometric inhibitors, and positive feedback. *Trends Biochem Sci* **39**(11), 556-569. (doi:10.1016/j.tibs.2014.09.003).

7. Ferrell J.E., Jr., Ha S.H. 2014 Ultrasensitivity part III: cascades, bistable switches, and oscillators. *Trends Biochem Sci* **39**(12), 612-618. (doi:10.1016/j.tibs.2014.10.002).

8. Carlstrom L.P., Hines J.H., Henle S.J., Henley J.R. 2011 Bidirectional remodeling of beta1-integrin adhesions during chemotropic regulation of nerve growth. *BMC Biol* **9**, 82. (doi:10.1186/1741-7007-9-82).

9. Iber D., Campbell I.D. 2006 Integrin activation--the importance of a positive feedback. *Bull Math Biol* **68**(4), 945-956. (doi:10.1007/s11538-005-9049-5).

10. Welf E.S., Naik U.P., Ogunnaike B.A. 2012 A spatial model for integrin clustering as a result of feedback between integrin activation and integrin binding. *Biophys J* **103**(6), 1379-1389. (doi:10.1016/j.bpj.2012.08.021).

11. Prehoda K.E., Scott J.A., Mullins R.D., Lim W.A. 2000 Integration of multiple signals through cooperative regulation of the N-WASP-Arp2/3 complex. *Science* **290**(5492), 801-806.

12. Malecka K.A., Szentpetery Z., Peterson J.R. 2013 Synergistic activation of p21-activated kinase 1 by phosphatidylinositol 4,5-bisphosphate and Rho GTPases. *J Biol Chem* **288**(13), 8887-8897. (doi:10.1074/jbc.M112.428904).

13. Zaidel-Bar R., Milo R., Kam Z., Geiger B. 2007 A paxillin tyrosine phosphorylation switch regulates the assembly and form of cell-matrix adhesions. *J Cell Sci* **120**(Pt 1), 137-148. (doi:10.1242/jcs.03314).

14. Goni G.M., Epifano C., Boskovic J., Camacho-Artacho M., Zhou J., Bronowska A., Martin M.T., Eck M.J., Kremer L., Grater F., et al. 2014 Phosphatidylinositol 4,5-bisphosphate

triggers activation of focal adhesion kinase by inducing clustering and conformational changes. *Proc Natl Acad Sci U S A* **111**(31), E3177-3186. (doi:10.1073/pnas.1317022111).

15. Stamatakis M., Mantzaris N.V. 2009 Comparison of deterministic and stochastic models of the lac operon genetic network. *Biophys J* **96**(3), 887-906. (doi:10.1016/j.bpj.2008.10.028).

16. Argiro V., Bunge M.B., Johnson M.I. 1984 Correlation between growth form and movement and their dependence on neuronal age. *J Neurosci* **4**(12), 3051-3062.

17. Szebenyi G., Callaway J.L., Dent E.W., Kalil K. 1998 Interstitial branches develop from active regions of the axon demarcated by the primary growth cone during pausing behaviors. *J Neurosci* **18**(19), 7930-7940.

18. Zelina P., Avci H.X., Thelen K., Pollerberg G.E. 2005 The cell adhesion molecule NrCAM is crucial for growth cone behaviour and pathfinding of retinal ganglion cell axons. *Development* **132**(16), 3609-3618. (doi:10.1242/dev.01934).

19. Mason C.A., Wang L.C. 1997 Growth cone form is behavior-specific and, consequently, position-specific along the retinal axon pathway. *J Neurosci* **17**(3), 1086-1100.

20. Halloran M.C., Kalil K. 1994 Dynamic behaviors of growth cones extending in the corpus callosum of living cortical brain slices observed with video microscopy. *J Neurosci* **14**(4), 2161-2177.

21. Godement P., Wang L.C., Mason C.A. 1994 Retinal axon divergence in the optic chiasm: dynamics of growth cone behavior at the midline. *J Neurosci* **14**(11 Pt 2), 7024-7039.

22. Skaliora I., Adams R., Blakemore C. 2000 Morphology and growth patterns of developing thalamocortical axons. *J Neurosci* **20**(10), 3650-3662.